Supplementary Information (SI) for Energy & Environmental Science.
This journal is © The Royal Society of Chemistry 2026

Supporting Information for

Breaking the Cascade Dissolution Loop through Self-inhibition Mechanism for Zinc Vanadium Oxide Battery

Weina Xu[1], Zimin Li[1], Kangjie Li[1], Huitong Lin[1], Shaobing Zhang[2], Ruohan Yu[3,*], Haoqing Ma[3], Liheng Zheng[3], Zijie Tang[4], Guobin Zhang[5,*], Jialun Guo[1], Fujia Zuo[1], Lei Zhang[3,*], Kangning Zhao[2,*]

[1] School of Materials Science and Engineering, Dongguan University of Technology, Guangdong 523808, P. R. China

[2] School of Physical Sciences, Great Bay University, Dongguan 523808, P. R. China

[3] Department of Materials Science and Technology, Wuhan University of Technology, Wuhan 430050, P. R. China

[4] Dongguan Amazinc Energy Limited, P. R. China

[5] Future Technology School, Shenzhen Technology University, Shenzhen, 518055 China

*Corresponding authors.

E-mail: yuruohan@whut.edu.cn (Ruohan Yu); whutzgb@163.com (Guobin Zhang); zhanglei1990@whut.edu.cn (Lei Zhang); vicyel@gbu.edu.cn (Kangning Zhao)

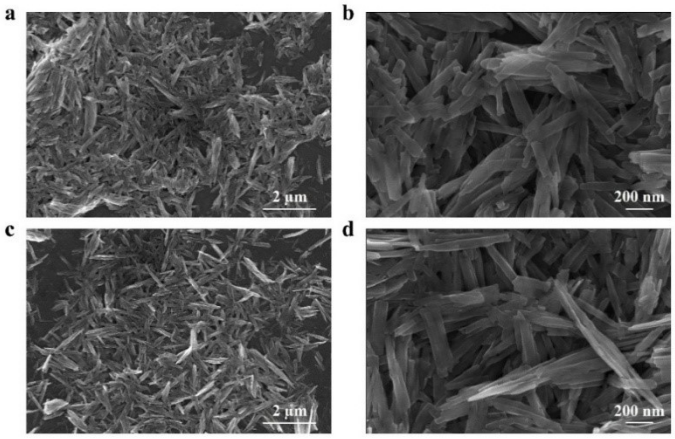

Fig. S1 SEM images of **a, b** VO_2 and **c, d** Ca-VO_2.

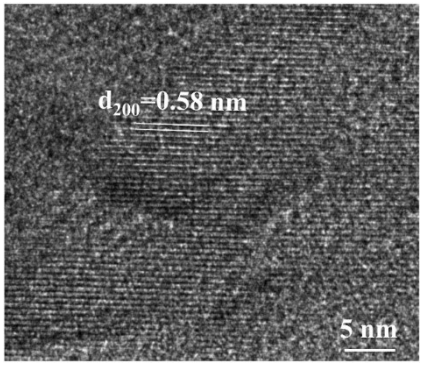

Fig. S2 HRTEM image of VO_2.

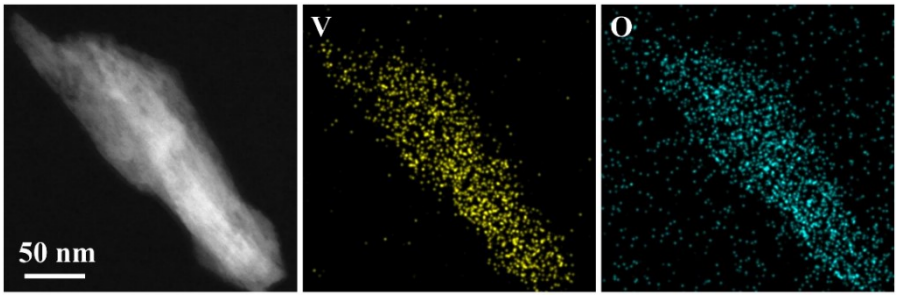

Fig. S3 HAADF-STEM image of VO_2 with corresponding elemental mapping.

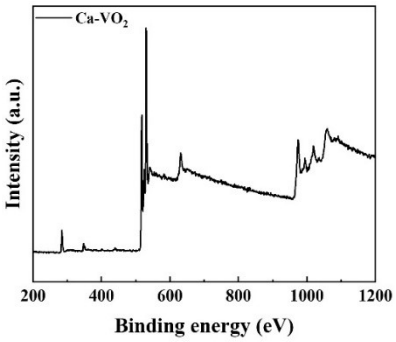

Fig. S4 XPS spectrum of Ca-VO_2.

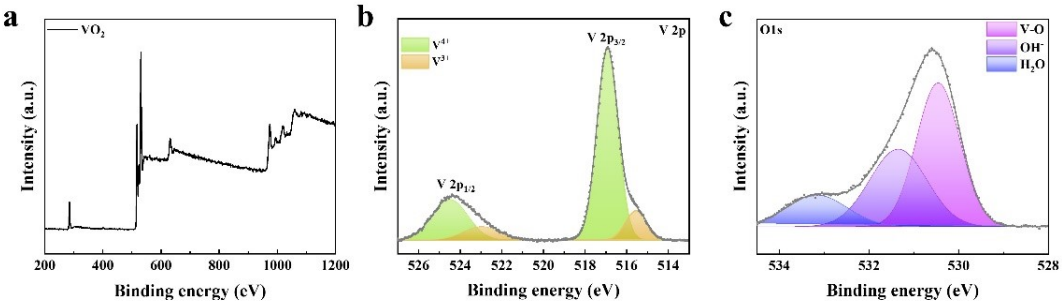

Fig. S5 a XPS spectrum of VO_2. **b** V 2p and **c** O 1s high-resolution XPS spectra.

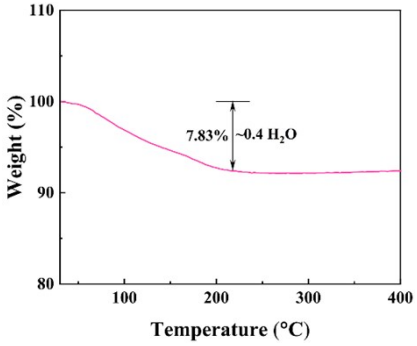

Fig. S6 TGA curve of Ca-VO_2.

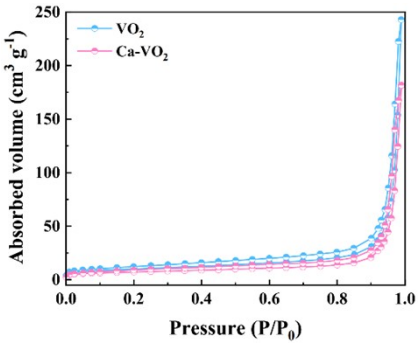

Fig. S7 BET surface area analysis of VO_2 and Ca-VO_2.

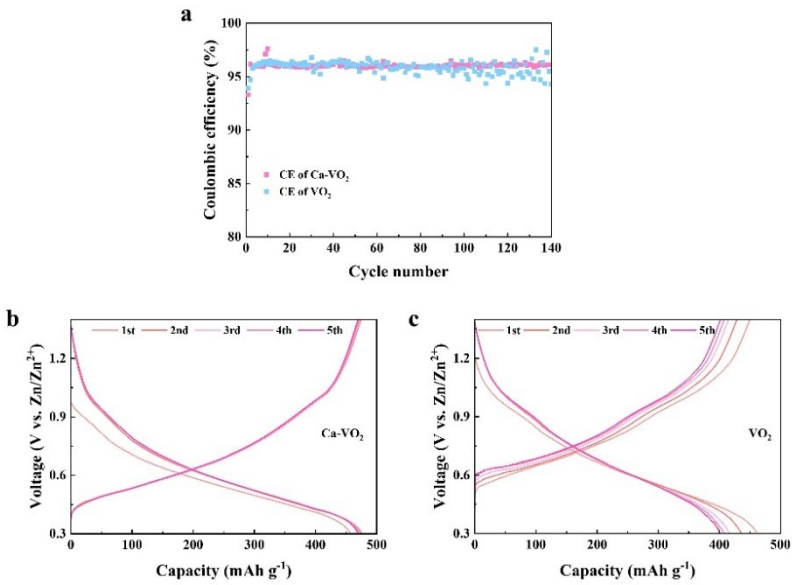

Fig. S8 a Coulombic efficiency of the Ca-VO_2 and VO_2 cathodes at 0.1 A g^{-1}. GCD curves of **b** Ca-VO_2 and **c** VO_2 at first five cycles at 0.1 A g^{-1}.

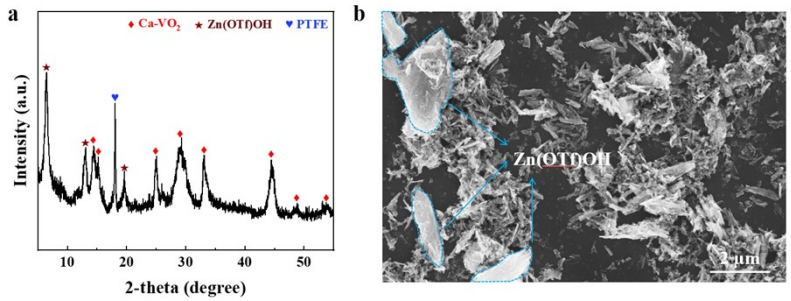

Fig. S9 a XRD pattern and **b** SEM of the Ca-VO_2 cathode after cycling at 0.1 A g^{-1}.

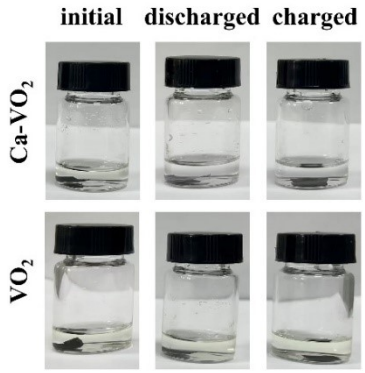

Fig. S10 The corresponding color variation for vanadium dissolution of the VO_2 and Ca-VO_2 electrodes in $Zn(OTf)_2$ electrolytes for 40 days at initial, discharged, and charged states.

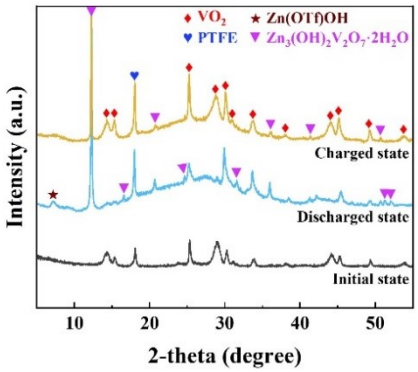

Fig. S11 XRD patterns of the VO_2 cathodes in initial, discharged and charged states.

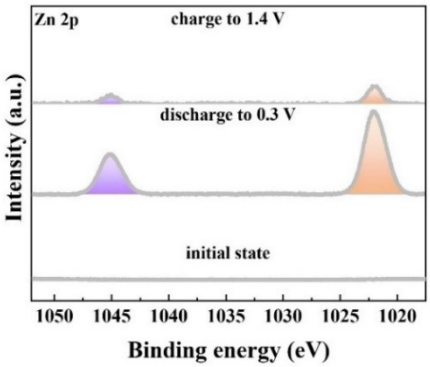

Fig. S12 *Ex-situ* XPS spectrum of Zn 2p in the Ca-VO_2 cathode at initial, discharged, and charged states.

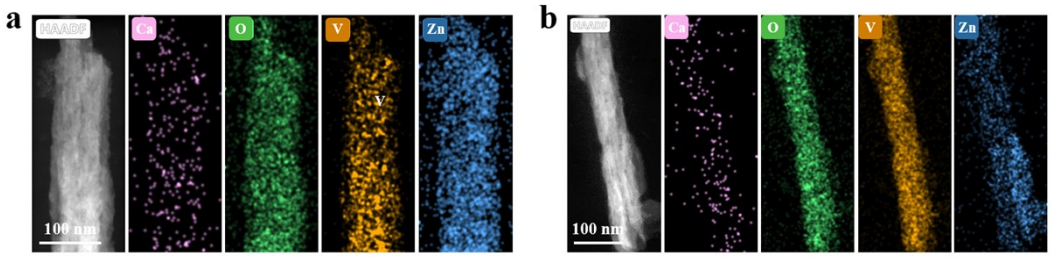

Fig. S13 The elemental mapping of the Ca-VO_2 cathodes at **a** discharged state and **b** charged state.

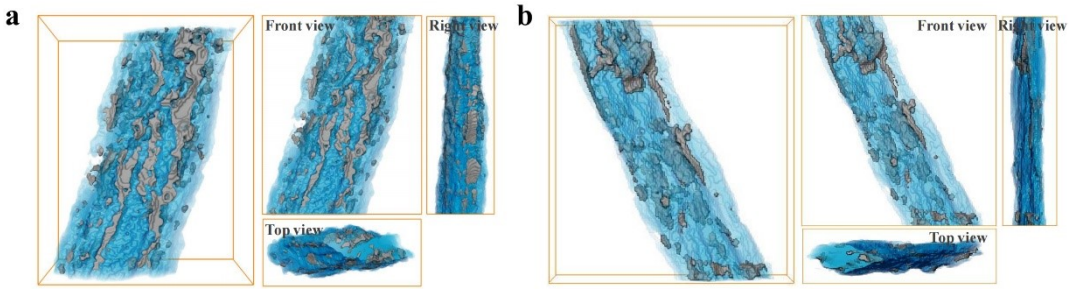

Fig. S14 The segmentation by contrast corresponding to Ca-VO_2 (blue) and a mixture of $CaV_2O_6 \cdot 2H_2O$ with Zn(OTf)OH (gray), and corresponding front, top, and right views for the reconstructed Ca-VO_2 nanorod at **a** the discharged state and **b** the charged state.

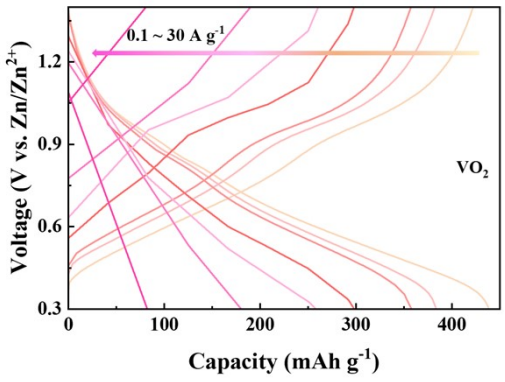

Fig. S15 GCD curves of the VO_2 cathode at different current densities increasing from 0.1 to 30 A g^{-1}.

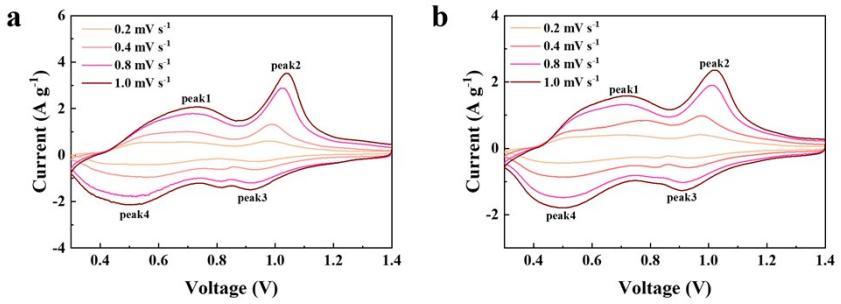

Fig. S16 CV curves of **a** Ca-VO_2 and **b** VO_2 cathodes at different scan rates.

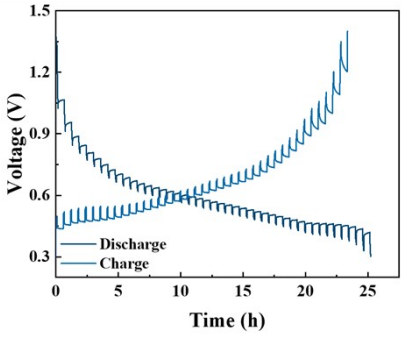

Fig. S17 GITT curve of the VO_2 cathode.

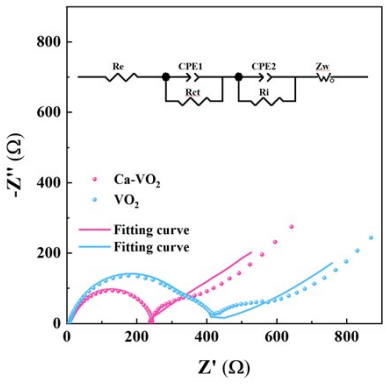

Fig. S18 Nyquist plots of the Ca-VO_2 and VO_2 cathodes. The inset is the equivalent circuit.

The EIS data are fitted using the equivalent circuit shown in the inset of Fig. S18, which consists of two constant phase elements (CPE_1 and CPE_2), ohmic resistance (R_e), charge transfer resistance (R_{ct}), interface resistance (R_i), and Warburg element (Z_W), respectively. And the fitting results are listed in Table S3.

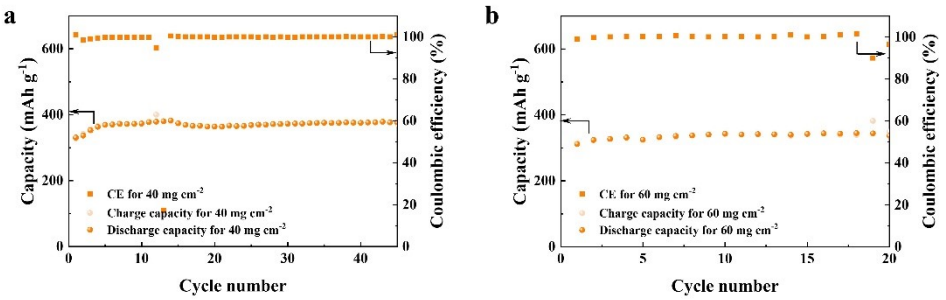

Fig. S19 Cycling performances of the Ca-VO_2 cathode at 0.1 A g^{-1} with high mass loadings: **a** 40 mg cm^{-2} and **b** 60 mg cm^{-2}.

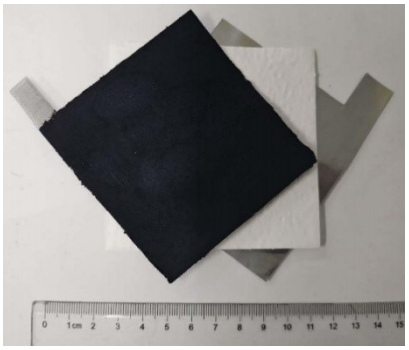

Fig. S20 Schematic diagram of the pouch cell configuration.

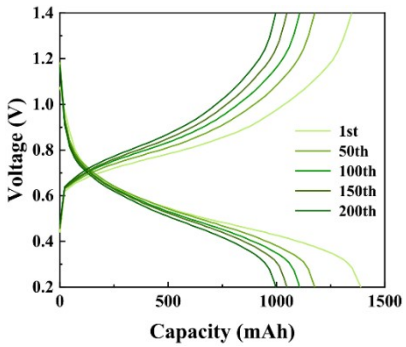

Fig. S21 GCD curves of Ca-VO_2/Zn pouch cell at selected cycles at 0.5 A g^{-1}.

Table S1. ICP-OES result of Ca-VO_2.

Element	Test solution element concentration [mg/L]	Element content W [%]
Ca	21.2267	2.07697
V	539.3050	52.7697

Table S2. A comparison of the long-term cycling performance between our as-prepared Ca-VO_2 cathode and current state-of-the-art vanadium-based cathodes for zinc-ion batteries.

Material	Electrolyte	Voltage [V]	Capacity/Current Density [mAh g^{-1}/A g^{-1}]	Capacity retention/ Cycle Performance	Refs.
VO_2(B)	3M $Zn(CF_3SO_3)_2$	0.2-1.5	344.8/10	84.3%/5000	[1]
Iodine-doped $Na_2V_6O_{16}\cdot 3H_2O$	3M $Zn(CF_3SO_3)_2$	0-1.6	289/10	74.9%/12000	[2]
$W_{0.05}V_{0.95}O_{1.94}$(B)	2M $Zn(CF_3SO_3)_2$	0.3-1.4	222/10	89%/2000	[3]
CaV_4O_9/CNTs	3M $Zn(CF_3SO_3)_2$	0.3-1.6	239/10	90.7%/3000	[4]
SWCNTs/GO/ $V_2O_5\cdot 1.6H_2O$	2M $Zn(CF_3SO_3)_2$	0.01-1.5	211.5/2	95.3%/3000	[5]
E-VON	2M $Zn(CF_3SO_3)_2$	0.2-1.5	155.5/10	73%/2500	[6]
VSSe/VO_2/V_2O_5	3M $Zn(CF_3SO_3)_2$	0.1-1.7	272/10	60%/12000	[7]
$Zn_{0.52}V_2O_5$-a·1.8 H_2O	3M $Zn(CF_3SO_3)_2$	0.2-1.6	161.5/20	95.4%/18000	[8]
D-VS_4	3M $Zn(CF_3SO_3)_2$	0.1-1.8	141/10	72%/8000	[9]
VO	2M $Zn(CF_3SO_3)_2$	0.2-1.6	133.3/50	97%/8000	[10]
$Na_6[V_{10}O_{28}]\cdot nH_2O$	2M $Zn(CF_3SO_3)_2$	0.2-1.5	84.6/10	89.7%/3000	[11]
V_2O_5	3M $Zn(CF_3SO_3)_2$	0.4-1.6	207/10	85%/5000	[12]
Rb-$NH_4V_4O_{10}$	3M $Zn(CF_3SO_3)_2$	0.2-1.6	152/5	87.6%/10000	[13]

V_2O_5@PEDOT	2M $Zn(CF_3SO_3)_2$	0.2-1.6	250/5	98.2%/2000	[14]
Ca-VO_2	**3M $Zn(CF_3SO_3)_2$**	**0.3-1.4**	**231.2/30**	**94.7%/16700**	**This work**

Table S3. Fitting results of the Nyquist plots for VO_2 and Ca-VO_2 cathodes.

Cathode	R_e [Ω]	R_{ct} [Ω]	R_i [Ω]
Ca-VO_2	6.03	222.30	72.89
VO_2	6.77	412.90	88.85

References

[1] Q. He, T. Hu, Q. Wu, C. Wang, X. Han et al., Tunnel-oriented VO_2(B) cathode for high-rate aqueous zinc-ion batteries. Adv. Mater. **36**, 2400888 (2024). https://doi.org/10.1002/adma.202400888

[2] X. Hu, S. Gao, T. Lin, X. Peng, Y. Huang et al., Iodine-doped sodium vanadate cathode for improved Zn ion diffusion kinetics. Adv. Mater. 2416714 (2025). https://doi.org/10.1002/adma.202416714

[3] Y. Zhang, L. Cui, F. Cui, Y. Huang, G. Zhang et al., Activating H_3O^+ intercalation chemistry in aqueous Zn-VO_2(B) batteries via tungsten doping and oxygen vacancies. Small **21**, 2501001 (2025). https://doi.org/10.1002/smll.202501001

[4] Y. Du, X. Wang, Y. Zhang, H. Zhang, J. Man, K. Liu, J. Sun, High mass loading CaV_4O_9 microflowers with amorphous phase transformation as cathode for aqueous zinc-ion battery. Chem. Eng. J. **434**, 134642 (2022). https://doi.org/10.1016/j.cej.2022.134642

[5] Z. Qin, G. Han, Y. Yang, S. Hao, L. Yu et al., Freestanding vanadium oxides/carbon hybrid cathode with long-term cyclability at low current density for flexible aqueous zinc ion batteries. Chem. Eng. J. **513**, 162952 (2025). https://doi.org/10.1016/j.cej.2025.162952

[6] Y. Xu, F. Shao, Y. Huang, X. Huang, F. Jiang et al., Ultra-fast activated $NH4^{+}$-intercalated vanadium oxide cathode for high-performance aqueous zinc-ion batteries. J. Colloid Interf. Sci. **683**, 226-235 (2025). https://doi.org/10.1016/j.jcis.2024.12.162

[7] M. Yang, Y. Lin, P. Chen, M. Lai, J. Zhu et al., Unlocking ultrafast-kinetics aAsymmetric heterojunction with multi-anionic redox chemistry enables high energy/power density and low-temperature zinc-ion batteries. Angew. Chem. Int. Edit. **64**, e202510907 (2025). https://doi.org/10.1002/anie.202510907

[8] W. Liang, D. Rao, T. Chen, R. Tang, J. Li, H. Jin, $Zn_{0.52}V_2O_{5-a}\cdot 1.8\ H_2O$ cathode stabilized by in situ phase transformation for aqueous zinc-ion batteries with ultra-long cyclability. Angew. Chem. Int. Edit. **61**, e202207779 (2022). https://doi.org/10.1002/anie.202207779

[9] F. Wu, Y. Wang, X. Dai, S. Meng, D. Zheng et al., Toward ultralong lifespan aqueous zinc-ion batteries via sulfur-defect vanadium tetrasulfide cathode. ACS Appl. Energy Mater. **6**, 2680-2686 (2023). https://doi.org/10.1021/acsaem.2c04102

[10] W. Qian, Z. Chen, L. Chen, Q. Sun, H. Zhou et al., Mixed-valence vanadium oxides with ultra-high rates and long cycles for aqueous zinc ion batteries. Appl. Surf. Sci. **684**, 161981 (2025). https://doi.org/10.1016/j.apsusc.2024.161981

[11] H. He, F.-C. Pan, X.-W. Liang, Q. Hu, S. Liu, et al., Unveiling the effect of structural water on Zn-ion storage of polyoxovanadate for high-rate and long-life

aqueous zinc ion battery. Chem. Eng. J. **462**, 142221 (2023). https://doi.org/10.1016/j.cej.2023.142221

[12] D. Chen, X. Rui, Q. Zhang, H. Geng, L. Gan et al., Persistent zinc-ion storage in mass-produced V_2O_5 architectures. Nano Energy **60**, (2019) 171-178. https://doi.org/10.1016/j.nanoen.2019.03.034

[13] K. Wang, S. Li, X. Chen, J. Shen, H. Zhao, Y. Bai, Trifunctional Rb^+-intercalation enhancing the electrochemical cyclability of ammonium vanadate cathode for aqueous zinc ion batteries. ACS nano **18**, 7311-7323 (2024). https://doi.org/10.1021/acsnano.4c00803

[14] Z. Li, Y. Liu, S. Yang, Z. Pan, C. Liu et al., Probing capacity decay in vanadium oxide cathodes of aqueous zinc-ion batteries using operando EQCM-D. ACS Energy Lett. **10**, 2821-2830 (2025). https://doi.org/10.1021/acsenergylett.5c00901